Published by IOP Publishing for Sissa Medialab

Received: *January 24, 2025*
Revised: *March 27, 2025*
Accepted: *June 2, 2025*
Published: *June 17, 2025*

Design and optimization of a liquid scintillator detector for new EAS hybrid experiment

Y. Zhang[a,*] **J. Huang**[a] **D. Chen**[b] **L.M. Zhai**[b] **Y. Meng**[a,c] **K.Y. Hu**[a,c] **Y.H. Zou**[a,c] **Y.L. Yu**[a,c] **and Y.Y. Li**[c]

[a] *State Key Laboratory of Particle Astrophysics, Institute of High Energy Physics, Chinese Academy of Sciences, 19B YuquanLu, Shijingshan District, Beijing 100049, China*
[b] *National Astronomical Observatories, Chinese Academy of Sciences, 20A Datun Road, Chaoyang District, Beijing 100012, China*
[c] *University of Chinese Academy of Sciences, No. 1 Yanqihu East Rd, Huairou District, Beijing, 101408, China*

E-mail: yingzhang@ihep.ac.cn

Abstract: The Stereoscopic Water Cherenkov Detector Array (SWCDA) is a Research and Development (R&D) project aiming to design a high-energy (HE) gamma-ray observatory sensitive to energy range from 100 GeV to hundreds of TeV. It aims to extend low energy to 100 GeV, connecting with satellite experiments (e.g. Fermi-LAT), and complements existing ground-based experiments (e.g. Tibet ASγ, HAWC and LHAASO) in the low energy region. It consists of liquid scintillator (LS) array and a stereoscopic water Cherenkov detector array. The stereoscopic water Cherenkov detector array is a ground-based experiment that innovates the observation of cosmic ray shower from the original plane observation to stereo observation. The stereo detector mainly observes the longitudinal distribution of cosmic rays and gamma-ray secondary particles in the atmosphere to do P/γ identification, and exclude the background of cosmic rays, while the LS detector is used to eliminate a large number of noise signals. For the LS detector, considering the portable and low-cost for future planning, the LS detector is composed of polymethyl methacrylate (PMMA) box used to contain LS, wavelength shifting (WLS) fibers, clear optical fibers used to collect and transmit the scintillation light and photomultiplier tube (PMT) used to convert the light signals into electrical signals. In this paper, the design and optimization of the LS detector are discussed in detail. The LS prototype experiment will be jointly run with the Tibet ASγ experiment in a hybrid array to test the performance.

Keywords: Detector design and construction technologies and materials; Scintillators, scintillation and light emission processes (solid, gas and liquid scintillators)

*Corresponding author.

https://doi.org/10.1088/1748-0221/20/06/P06017

Contents

1 Introduction

The observation of high-energy gamma rays (HE gamma rays: 20 MeV–30 TeV) is closely related to the astronomical phenomena such as double neutron-star merger, cosmic-ray accelerators, galactic supernova, active galactic nucleus (AGN), etc. Satellite experiments represented by the Fermi Gamma-ray Space Telescope have achieved great success in gamma-ray observations in the MeV-GeV energy region [1, 6], but they are powerless above 100 GeV because of limited exposure time and small detective area. So the task of HE gamma-ray observations relies on the ground-based indirect measurements due to the large area, high duty cycle, and wide field of view, such as the Tibet ASγ [4], the HAWC [2], and the LHAASO [7]. With the experimental development in recent years, the observational sensitivity in the energy range above tens of TeV has been significantly improved, even background-free observations have almost been achieved above 100 TeV. However, these ground-based extensive air shower (EAS) experiments still face some shortcomings in the TeV energy range, such as relatively low cosmic-ray background rejection rate (~96%@TeV), poor angular resolution (about 1°@TeV), and high energy threshold (~ a few hundred GeV). For the 100 GeV to 1 TeV energy region, the current ground EAS experiments are almost blank.

The Stereoscopic Water Cherenkov Detector Array (SWCDA) is a Research and Development (R&D) project aiming to design a HE gamma-ray observatory sensitive to energy range from 100 GeV to hundreds of TeV. The science goals include continuous observation of HE gamma-ray sources and transients such as Blazars and Gamma-Ray Burst (GRBs), etc. With these objectives, SWCDA is designed with a low energy threshold and a wide field-of-view of about 2 sr, at a very high altitude,

and combines liquid scintillator (LS) array and a stereoscopic water Cherenkov detector array. The stereo detector mainly observes the longitudinal distribution of cosmic rays and gamma-ray secondary particles in the atmosphere to do P/γ identification, and exclude the background of cosmic rays, while the LS is used to eliminate a large number of noise signals. In this paper, we focus on introduce the development and design of LS detector only.

LS is widely used in particle physics experiments due to its advantages such as high light yield, fast response time, good energy resolution, and tunable chemical properties. In the KASCADE experiment, the LS detector works in conjunction with scintillator array to detect secondary particles in cosmic ray air showers [5]. In the SWCDA project, the LS detector's primary role is to measure charge and time information of secondary particles, enabling the rejection of a large fraction of background events and thereby lowering the threshold of primary cosmic rays. For high-energy gamma-ray bursts, secondary particles include low-energy electrons and photons, which are critical for lowering the detection threshold and improving background rejection. LS detectors, with their high light yield and good energy resolution, are particularly effective in this low-energy regime, complementing the capabilities of water Cherenkov detectors.

For the LS detector, considering the portable and low-cost for future planning which will make it more convenient to manufacture, we plan to carry out the development of polymethyl methacrylate (PMMA) box used to contain LS, wavelength shifting (WLS) fibers, clear optical fibers used to collect and transmit the scintillation light and photomultiplier tube (PMT) used to convert the light signals into electrical signals. The LS prototype experiment will be operated in conjunction with the Tibet ASγ experiment as part of a hybrid array to test the performance.

In this paper, we first introduce the design of LS detector in section 2. Then, the optimization tests have been studied in detail in section 3. In section 4, we discuss the performance characteristics of the LS detector. Finally, section 5 concludes the paper with a summary.

2 Experiment

2.1 Principle of the LS detector

The structure of LS detector consists of LS, a PMMA container, fibers and a PMT. These components work in unison to facilitate the efficient detection and measurement of high-energy particles. Below are the principles of each component of the detector.

- LS: liquid scintillator is the core medium of the detector, responsible for converting the energy of high-energy particles into fluorescent photons. When high-energy particles (such as neutrons, gamma rays, or charged particles) interact with LS, the solvent molecules in the scintillator are excited and then transfer energy to the scintillating solutes (e.g., PPO), which then emit fluorescent photons.
- PMMA box: the container box is designed to hold the LS and provides mechanical support and optical interfaces. PMMA has been selected as the container material due to its low radioactivity and high transparency, in order to reduce background noise and ensure efficient light transmission.
- Fiber: optical fibers are crucial for light transmission within the detector, transporting the fluorescent photons generated in the LS to the PMT. There are two types of optical fibers used: wavelength shifting (WLS) fibers and clear optical fibers. WLS fibers convert short-wavelength fluorescent photons into longer-wavelength photons, while clear optical fibers efficiently transmit light to the PMT.

2025 JINST 20 P06017

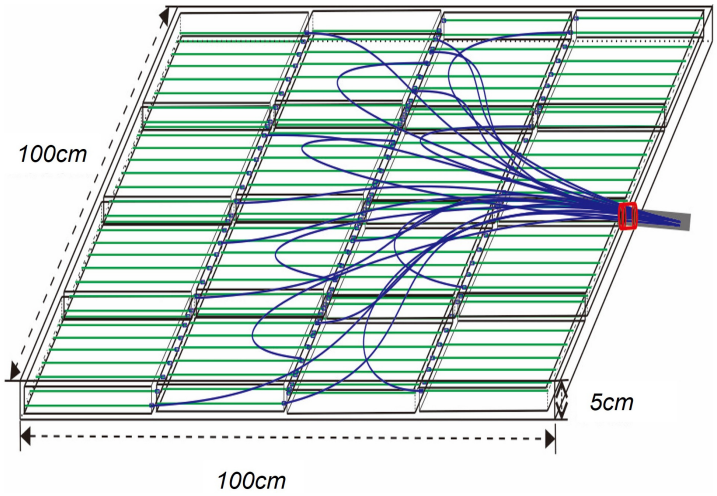

Figure 1. The schematic view of LS detector. Each LS detector consists of 1 m^2 liquid scintillator, WLS fibers, clear optical fibers, and a photomultiplier tubes (PMT). Fibers are equally spaced along the sides of the PMMA container to ensure uniform light collection.

- PMT: PMT serves as the signal conversion component of the detector, responsible for converting fluorescent photons into electrical signals.

2.2 Design of the LS detector

The design of a LS detector should comprehensively consider the optical, mechanical performance of each component while also balancing cost, size, and weight. Based on MC simulations, we designed the structure of each LS detector consisting of 1 m^2 LS, along with wavelength shifting (WLS) fibers, clear optical fibers, and a PMT, as shown in figure 1. The LS with an area of 1 m^2 is divided into 16 small units contained in PMMA box whose size is 25 cm × 25 cm × 5 cm (length × width× thickness). Scintillation light is collected by using double cladded fibers, which include both WLS fibers and clear optical fibers. The WLS fibers with a diameter of 1.5 mm are placed in the slots of a PMMA plate beneath the container. Fibers are equally spaced along the sides of the PMMA container to ensure uniform light collection. One end of each WLS fiber is plated with aluminum for the reflection, while the other end is connected to clear optical fibers. Compared with an air guide, the use of optical fibers can reduce the overall volume of detector, as well as improve light collection uniformity. The clear optical fibers are attached to a PMT for readout. Each small unit is wrapped with a layer of Tyvek sheet to improve photon collection efficiency and then covered with a black mask to avoid external and inter optical crosstalk on the outermost. PMT is used to convert the light signals into electrical signals, which are then amplified, processed, and recorded by subsequent electronic systems.

3 Optimization of the LS detector

In order to eliminate a large number of noise signals as trigger system, it is necessary to measure the number of shower particles after passing through each LS detector.In fact, the design of each component of the detector will affect the final photon output, such as the thickness of LS, the quantity and layout of the fibers, PMT performance, container reflectivity and others. In this section, the main optimized design of the LS detector is described in detail.

2025 JINST 20 P06017

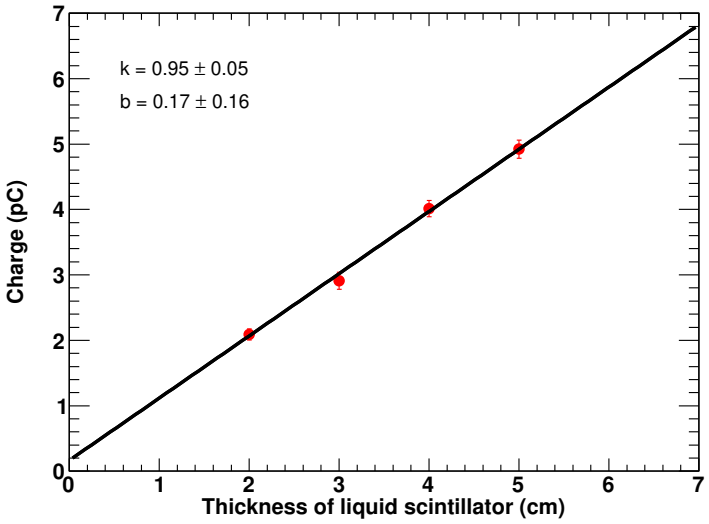

Figure 2. The correlation between the charge output and the thickness of liquid scintillator.

3.1 Optimization of LS

3.1.1 Affected by LS thickness

When charged particles passed through the LS, the quantity of scintillation light depends on the energy deposits, which is in proportion to the length of MIP's (Minimum Ionization Particle) track in the detector. Consequently, the linearity of charge output versus the thickness of LS is measured. The resolution of the analog-to-digital converter (ADC) is 0.25 pC/count. Figure 2 shows the correlation between the charge output and the thickness of LS, which can be fitted with a linear function $y = k \cdot x + b$ with k and b to be determined from the experimental measurements. The black solid circles denote the experimental data, while the red solid line denotes the best fit result by the linear function. The error bars on the plot represent statistical uncertainties. The fitted slope is k=0.95±0.05 and the intercept is b=0.17±0.16. The intercept b is statistically compatible with zero within its 1σ uncertainty, suggesting no significant deviation from linearity under the experimental condition, which supports the validity of the linear model for describing the relationship between charge output and LS thickness.

3.1.2 Affected by temperature variation

Compared with plastic scintillators, LS is more sensitive to temperature variation, especially the LS detector array will be built in Yangbajing with large temperature difference within one year even one day. Therefore, we used a temperature-controlled chamber to measure how the light yield of LS varies with temperature. Figure 3 shows the relationship between relative light yield and temperature of LS. The vertical axis denotes the ratio of light yield at different temperature to that obtained at 0°. The black solid circles denote the experimental data with the errors representing statistical uncertainties. The red solid line denotes the best fit result by the linear function $y = k \cdot x + b$. The slope of the linear fit to the data is k=-0.0023, with an uncertainty of 0.0002. It can be found that the effect of temperature changes on the light output of LS based on Linear Alkylbenzene (LAB) is less than 20% in a range from -32°C to 40°C. In fact, the prototype array will perform a real-time calibration every 20 minutes during the data acquisition similar to the Tibet ASγ experiment [3]. Therefore, the variation of light yield emitted by LS with temperature changes can meet our requirements.

2025 JINST 20 P06017

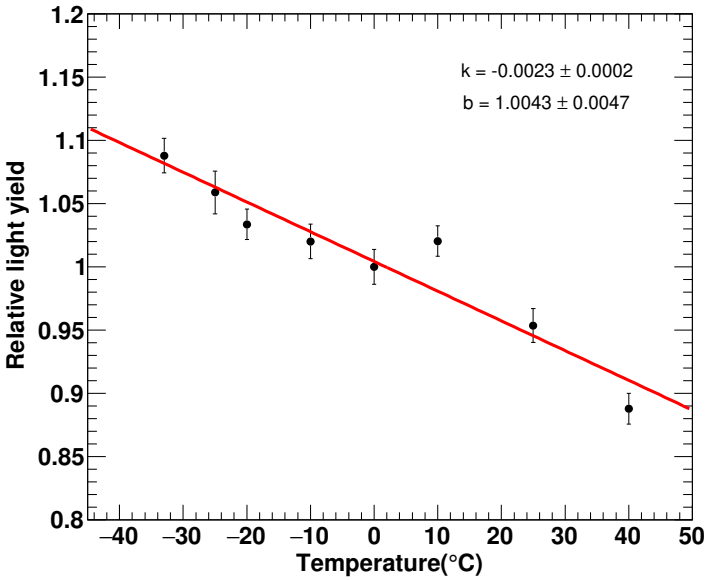

Figure 3. The relationship between relative light yield and temperature of LS. Data was normalized with respect to 0°.

However, due to the thermal expansion and contraction effects of LS, we also need to consider the design of an overflow device for the detector. Firstly, we filled the PMMA box (25 cm × 25 cm × 5 cm) at -32°, and then placed it in a room temperature environment. We found that with a temperature variation of 55°, the volume of LS expansion was approximately 75 milliliters. According to the 0.055% temperature coefficient of the LS formula, the theoretically calculated LS expansion volume is about 81 milliliters. The experimental results are consistent with the theoretical calculations with a relative deviation of 7.4%, indicating that the expansion behavior of the LS is within expectations. To accommodate this expansion, we drilled a hole in the upper surface of the PMMA box and installed a connector along with a 150-milliliter plastic bag to serve as an overflow device for the detector, as shown in the figure 4. Additionally, we also tested the selected connector and plastic bag and confirmed that they caused almost no contamination to the LS, thereby meeting the experimental requirements.

3.2 Optimization of fiber scheme

In LS detectors, optical fibers play a crucial role in collecting and transmitting light, making the optimization of fiber design very important. There are many approaches to achieve optimization goals, such as adjusting quantity of fibers to balance cost and performance, optimizing the arrangement of fibers to improve light collection efficiency and uniformity, or enhancing the coupling between fibers to minimize light loss. During the optimization process, we first determined the optimal number of fibers based on a fixed placement configuration. Then, with the number of fibers fixed, we optimized their placement. Finally, with the number of fibers and their placement fixed, we evaluated the effect of different coupling methods on light transmission efficiency. The followings are the results of the specific optimization tests.

2025 JINST 20 P06017

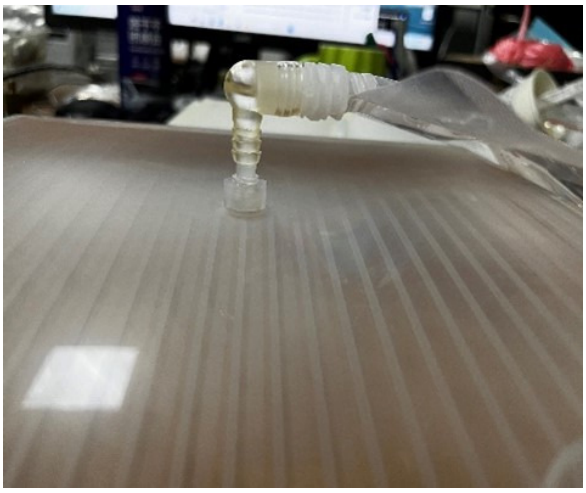

Figure 4. The LS overflow device for the detector.

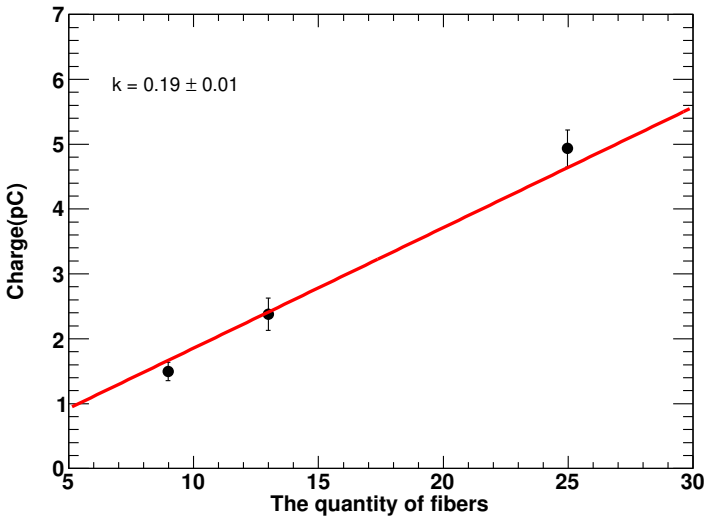

Figure 5. The charge output of LS detector varies linearly with the quantity of fibers.

3.2.1 Affected by fiber quantity

As we know, the amount of scintillation light collected is influenced by the quantity of optical fibers used. Therefore, the linearity of the quantity of fibers is tested. This step aimed to establish the baseline dependence of light collection on fiber quantity under fixed fiber placement and coupling condition. Figure 5 shows the resultant charge output of LS detector versus the quantity of fibers. The error bars on the plot represent statistical uncertainties. The solid red line denotes the best fit result by a linear function $y = k \cdot x$. The slope of the linear fit to the data is $k = 0.19 \pm 0.01$. In fact, we also fitted the data to a linear plus a quadratic term. The results indicate that the linear model sufficiently describes the data, and the inclusion of a quadratic term does not yield a statistically significant improvement. The linear relationship not only indicates our testing system has no issues, but also provides an important reference for the design of the detector with the combined parameters such as the thickness of LS.

2025 JINST 20 P06017

Figure 6. (1) placing the fibers in the slots of a PMMA plate beneath the container, (2) placing the fibers in the slots of a PMMA plate on the side of the container.

3.2.2 Affected by fiber placement

Changing the position of WLS fibers in the detector will result in different numbers of photoelectrons, indicating that the photon collection efficiency depends on the coupling position between the fibers and the scintillator. We tested the following configurations: (1) placing the fibers in the slots of a PMMA plate beneath the container; (2) placing the fibers in the slots of a PMMA plate on the side of the container, as shown in figure 6. In both configurations, the number of fibers used remains the same by adjusting the spacing between the fibers. The fibers are placed equidistant along the sides of the LS detector to ensure uniform light collection. The test results show that placing the fibers in the slots of a PMMA plate beneath the container can improve light collection efficiency by approximately 20%. This allows us to adopt the first configuration, thereby effectively enhancing photon collection efficiency.

3.2.3 Affected by fiber coupling

To further improve light collection efficiency, we tested various coupling methods for WLS fibers and clear fibers, aiming to minimize light loss caused by fiber connections. During this testing process, the number of optical fibers were fixed which are uniformly positioned in the slots of a PMMA plate beneath the container, consistent with the final detector configuration. The different fiber coupling methods included air coupling, coupling with BC-600 epoxy resin produced by Saint-Gobain, coupling with acrylic resin produced by QUINSON company, and coupling with 502 Cyanoacrylate adhesive. The test results showed that, comparing to the scenario without fiber connections, the light yield using Saint-Gobain BC-600 epoxy resin and QUINSON acrylic resin was 70% of the original, while the 502 adhesive method achieved 66%, and the air coupling method yielded 60%, as can be seen in table 1. Uncertainties in light yield (±5%) account for PMT gain drift, fiber alignment variations, and environmental fluctuations. While 502 cyanoacrylate adhesive exhibited slightly lower light yield (66% ± 5%) compared to epoxy resins (70% ± 5%), it was selected as the preferred method for fiber coupling due to its rapid curing time, field durability under mechanical stress, and compatibility with assembly timelines. Operational convenience here refers to minimizing setup complexity and ensuring robustness in harsh environments. Safety hazards were mitigated through mandatory protective equipment (gloves, goggles) and ventilation protocols during installation.

2025 JINST 20 P06017

Table 1. Different coupling methods for WLS fibers and clear fibers.

Coupling method	Charge output(pC) ± uncertainty (±5%)	Normalization
Air coupling	12.70 ± 0.64	60±4%
BC-600 epoxy resin	14.83 ± 0.74	70±5%
Acrylic resin	14.81 ± 0.74	70±5%
502 Cyanoacrylate adhesive	13.98 ± 0.70	66±5%

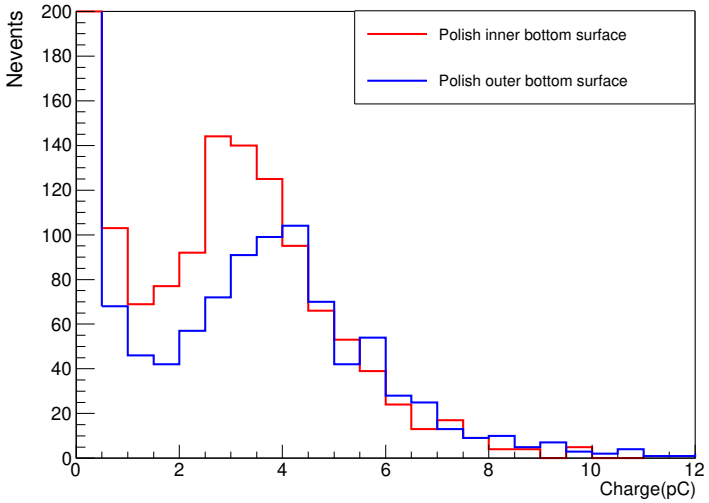

Figure 7. The output charge of polishing the inner (red line) and outer (blue line) bottom surfaces of the PMMA container.

3.3 Optimization of PMMA box

The LS will be contained in PMMA box which should provide excellent optical transparency and mechanical stability. The container design must consider sealing to prevent LS leakage or contamination, while also optimizing its boundary to maximize light collection efficiency. We used 3000-grit sandpaper to polish the inner and outer bottom surfaces of the PMMA container, respectively. From figure 7, we found that compared to polishing the inner bottom surface (red line), polishing the outer bottom surface (blue line) can reduce light reflection and increase light transmittance, thereby improving the light output by approximately 18%.

3.4 Selection of PMT

In the LS detector design, all fiber ends are connected to one PMT, making the performance of PMT critical to the overall performance of the detector. In this work, the charge measurement for LS detector covering a wide dynamic range is important. Two kinds of PMTs: North Night Vision Science Technology Research N2014 and HAMAMATSU R4125 have been studied. The linearity of each PMT is measured by LED light source and optical filters. In the test, the light intensity is varied by adjusting different intensity of filter. Figure 8 shows the response of the PMT versus the relative intensity of LED light respectively, which can be fitted with a function $y = a \cdot x^b$. The red solid circles denote the experimental data, while the black solid line denotes the best fit result by the linear function. In fact, the nonlinearity observed in figure 8 is not only originated from the PMT

2025 JINST 20 P06017

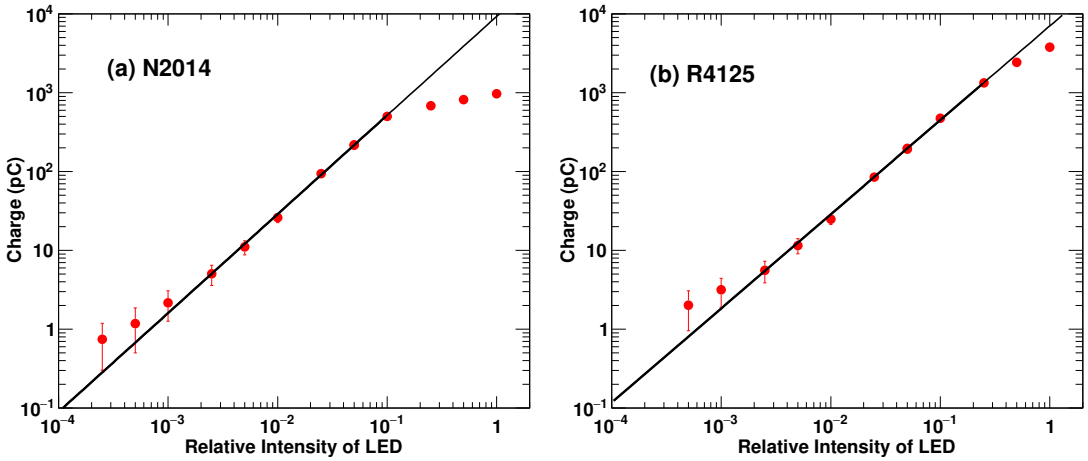

Figure 8. The response of PMTs: (a) N2014; (b)R4125 versus the relative intensity of LED light.

itself, but also be influenced by the light source (LED) and the readout system. The systematic error is about 7%. From this figure, we found that R4125 PMT has a wider dynamic range with a half order of magnitude within 7% systematic uncertainty, making it more suitable for our requirements. Additionally, due to the higher quantum efficiency of R4125, this model of PMT also exhibits better photoelectric conversion efficiency, resulting in higher photon collection efficiency.

4 Performance of the LS detector

4.1 Finalization of LS detector

After a series of optimized designs, and taking into account both cost and performance, we have determined that an appropriate configuration for the LS detector consists of a 1 m^2 LS area which is divided into 16 small units whose size is 25 cm×25 cm×5 cm, as shown in figure 9. Each small unit is equipped with LS overflow device and wrapped with a layer of Tyvek sheet to improve photon collection efficiency.The scintillation light is collected by using double-cladded fibers, 54 cm-long WLS fibers (BCF92) and 234 cm-long clear optical fibers (CK-60). The spacing between the fibers is 1.25 cm. A total of eighty WLS fibers, each with a diameter of 1.5 mm diameter, have been placed in the slots of a PMMA plate beneath the container. One end of these fibers is plated with aluminum for the reflection. The other ends are connected to clear optical fibers using 502 Cyanoacrylate adhesive. The eighty clear optical fibers are then attached to an R4125 PMT for readout. Considering the large temperature difference in Yangbajing, a heat-insulator layer is used inside each detector box.

4.2 Performance of charge measurement

As mentioned above, the LS detector is used to eliminate a large number of noise signals as trigger system, it is necessary to know the PMT output(charge) of a single-particle (SP) in each LS detector correctly. This can be determined by a probe calibration using cosmic rays, typically vertical single muons. We put a reference small detector (probe detector) which consists of a PMT (HAMAMATSU H1949) and a scintillator plate on top of the LS detector. When a charged particle punches through both the probe detector and the LS detector (the probe detector issues a trigger signal), the signal charge from the PMT corresponding to the energy deposit in LS detector is measured. Figure 10 shows

2025 JINST 20 P06017

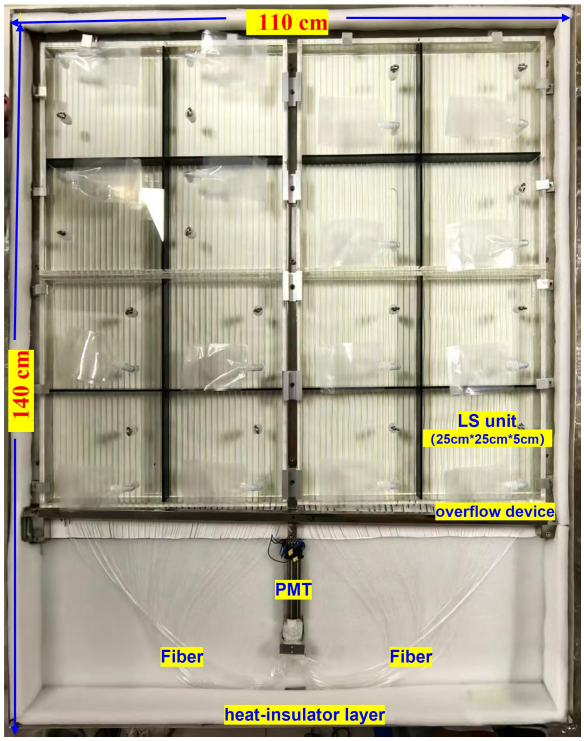

Figure 9. View of the LS detector. The LS detector with an area of 1 m^2 LS is divided into 16 small units whose size is 25 cm × 25 cm × 5 cm. Each small unit is equipped with LS overflow device. The scintillation light is collected by using double cladded fibers, 54 cm-long WLS fibers (BCF92) and 234 cm-long clear optical fibers (CK-60). The separation between fibers is 1.25 cm. A heat-insulator layer is used inside each detector box.

the photoelectrons (PEs) distribution of a single particle. The red solid circles denote experimental data and the black solid line is the fitting result to the PEs distribution by landau distribution. In this figure, the spike at 0 PE arises from background signals and the most probable value (MPV) of the photoelectron yield is measured as 15.58±0.14 PEs, with a standard deviation (σ) of 3.02±0.14. This corresponds to a resolution of 19.40±0.89%, calculated as the ratio of σ to the MPV which meets our requirements. We further investigated the systematic uncertainties during the probe calibration which mainly arise from the following sources: 1) errors due to position-dependent variation of the probe detector. When the probe detector is placed at different positions on the LS detector, the charged particles pass through the scintillator on different positions. This leads to slight variations in optical fiber transmission paths and transmitted to the PMT, which is less than 10%; 2) errors due to temperature effects. temperature shifts (±2°) in the lab can impact the light yield of single particles, which will contribute a systematic uncertainty of less than 1%; 3) errors due to electronic readout circuit which is less than 5%. The total systematic uncertainty is then estimated to be about 11%.

4.3 Performance of time measurement

We can also measure the time performance of LS detector by using the above probe calibration system. Single muon signals are selected by choosing coincident events between the top probe detector and down LS detector. The time resolution is measured from the time of flight (TOF) distribution of vertical single muons between probe detector and LS detector. Figure 11 shows the TOF distribution

2025 JINST 20 P06017

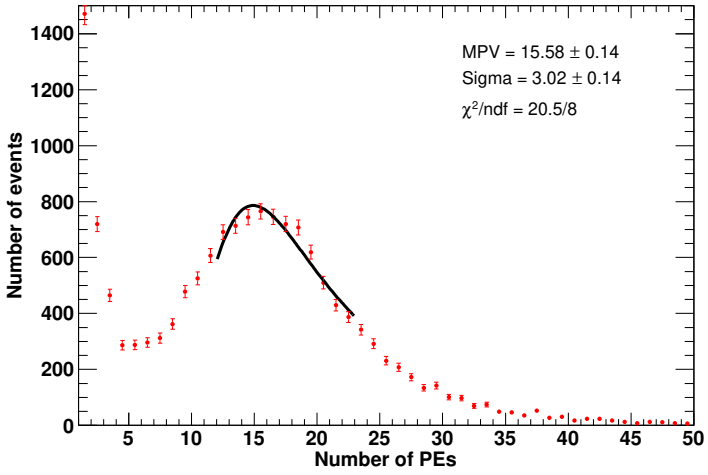

Figure 10. The photoelectrons (PEs) distribution of a single particle measured by LS detector.

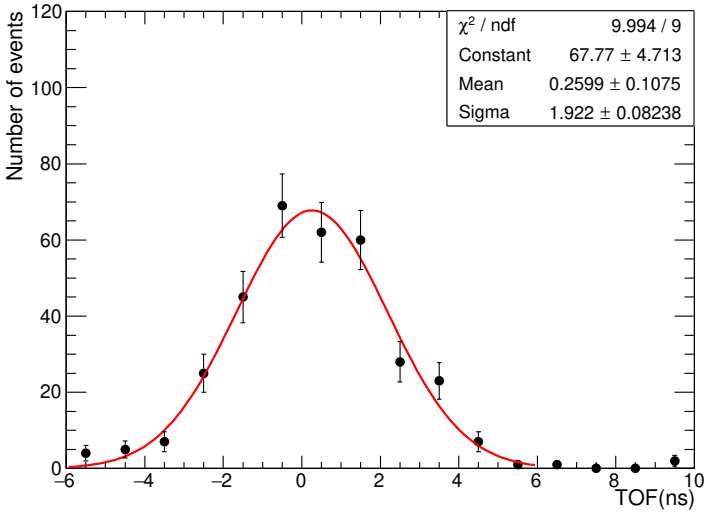

Figure 11. The time of flight (TOF) distribution of vertical single muons between probe detector and LS detector.

which obeys a Gaussian distribution. The time resolution of LS detector (σ) with vertical muons is found to be better than 2 ns. In fact, the measured time resolution σ includes contributions from both the LS detector (σ_{LS}) and the probe detector (σ_{probe}) which can be calculated as: $\sigma^2 = \sigma^2_{\mathrm{probe}} + \sigma^2_{\mathrm{LS}}$.The contribution of the probe detector can be measured independently using a known pulsed light source, where σ_{probe} is determined to be 1.0 ns. Therefore, we derive σ_{LS} with a value of 1.7 ns which confirms that the LS detector's intrinsic time resolution dominates the measurement.

5 Summary

In summary, considering the portable and low-cost for future planning, we have designed and optimized the LS detector. We tested the performance of various components of the detector to achive the goal, such as the thickness of LS, fiber quantity and layout scheme, PMT performance, container reflectivity and others. Ultimately, we determined that an optimal design for the LS detector with an area of 1 m^2

2025 JINST 20 P06017

is divided into 16 units contained in PMMA box whose size is 25 cm × 25 cm × 5 cm. The scintillation light is collected by using double-cladded fibers, 54 cm-long WLS fibers (BCF92) and 234 cm-long clear optical fibers (CK-60). A total of eighty WLS fibers have been placed in the slots of a PMMA plate beneath the container. The spacing between fibers is 1.25 cm. A prototype of the LS detector will operate in conjunction with the Tibet ASγ experiment as part of a hybrid array to test the performance.

Acknowledgments

The authors would like to express their thanks to the members of the Tibet ASγ collaboration for fruitful discussions. This work is supported by the National Natural Science Foundation of China (No. 12227804) and by the Key Laboratory of Particle Astrophysics at the Institute of High Energy Physics of the Chinese Academy of Science. Y. Zhang is supported by the National Natural Science Foundation of China (No. 12275282).

References

[1] Fermi-LAT collaboration, *Fermi Large Area Telescope First Source Catalog*, *Astrophys. J. Suppl.* **188** (2010) 405 [arXiv:1002.2280].

[2] A.U. Abeysekara et al., *HAWC observations of the acceleration of very-high-energy cosmic rays in the Cygnus Cocoon*, *Nature Astron.* **5** (2021) 465 [arXiv:2103.06820].

[3] Tibet ASγ collaboration, *Multi-TeV gamma-ray flares from Markarian 421 in 2000 and 2001 observed with the Tibet Air Shower Array*, *Astrophys. J.* **598** (2003) 242 [astro-ph/0304241].

[4] Tibet ASγ collaboration, *First Detection of Photons with Energy Beyond 100 TeV from an Astrophysical Source*, *Phys. Rev. Lett.* **123** (2019) 051101 [arXiv:1906.05521].

[5] A. Haungs et al., *The KASCADE Cosmic-ray Data Centre KCDC: Granting Open Access to Astroparticle Physics Research Data*, *Eur. Phys. J. C* **78** (2018) 741 [arXiv:1806.05493].

[6] Fermi-LAT collaboration, *Fermi Large Area Telescope Second Source Catalog*, *Astrophys. J. Suppl.* **199** (2012) 31 [arXiv:1108.1435].

[7] LHAASO collaboration, *A tera-electron volt afterglow from a narrow jet in an extremely bright gamma-ray burst*, *Science* **380** (2023) adg9328 [arXiv:2306.06372].

2025 JINST 20 P06017